Interacting Stark localization dynamics in a three-dimensional lattice Bose gas

Laura Wadleigh, Nicholas Kowalski, and Brian DeMarco

Phys. Rev. A **107**, 043325 — Published 28 April 2023

DOI: 10.1103/PhysRevA.107.043325

Interacting Stark localization dynamics in a three-dimensional lattice Bose gas

Laura Wadleigh, Nicholas Kowalski, and Brian DeMarco
Department of Physics, University of Illinois Urbana-Champaign, Urbana, Illinois 61801, USA
(Dated: April 4, 2023)

We measure the thermalization dynamics of a lattice Bose gas that is Stark localized by a parabolic potential. A non-equilibrium thermal density distribution is created by quickly removing an optical barrier. The resulting spatio-temporal dynamics are resolved using Mardia's B statistic, which is a measure sensitive to the shape of the entire density distribution. We conclude that equilibrium is achieved for all lattice potential depths that we sample, including the strongly interacting and localized regime. However, thermalization is slow and non-exponential, requiring up to 500 tunneling times. We show that the Hubbard U term is not responsible for thermalization via comparison to an exact diagonalization calculation, and we rule out equilibration driven by lattice-light heating by varying the laser wavelength. The thermalization timescale is comparable to the next-nearest-neighbor tunneling time, which suggests that a continuum, strongly interacting theory may be needed to understand equlibration in this system.

I. INTRODUCTION

Localization in many-particle quantum systems is an intense topic of active research [1–3]. Work in this area involving ultracold quantum gases has primarily focused on localization arising from disorder, interactions, and the interplay between the two [1–3]. Another less explored source of localization is a potential gradient, which acts through the Wannier–Stark effect in lattice systems [4]. In this scenario, localization arises solely from energy shifts between sites that are comparable to the lattice bandwidth. The influence of many-particle quantum effects and inter-particle interactions on Stark localization is an open question.

Recent numerical studies have probed Stark localization in interacting spin [5] and lattice models [2, 6–8], including the connection to many-body localization (MBL). For lattice systems, the transition between ergodic behavior and MBL for increasing potential gradient has been shown in energy level statistics for spinless fermions [6] and the Bose-Hubbard model in 1D [2]. Furthermore, logarithmic entropy growth consistent with MBL was found for an interacting fermionic system with nearest-neighbor interactions in one dimension [7]. Work in higher dimensions has been limited; studies have revealed Stark localization in two dimensions for hard-core bosons at higher gradients compared to the one-dimensional case [8].

There have been few experimental observations of interacting Stark localization. A chain of ions with long range spin–spin coupling has displayed a lack of thermalization and slow propagation of correlations in the presence of a linear potential gradient [9]. Interacting Stark localization has also been observed in a chain of transmon superconducting qubits [10] and in a quantum-gas tilted 1D Fermi-Hubbard model [11]. In a 2D Fermi-Hubbard lattice gas, applying a large potential gradient along one direction generated sub-diffusive behavior and slow dynamics [12].

We measure interacting Stark localization dynamics in a three-dimensional lattice Bose gas. Ultracold ^{87}Rb atoms are trapped in a cubic optical lattice, which (in the tight-binding limit) realizes the Bose-Hubbard model:

$$H = -t\sum_{\langle i,j\rangle}(\hat{b}_i^\dagger \hat{b}_j + h.c) + \sum_i \frac{U_i}{2}\hat{n}_i(\hat{n}_i - 1) + \sum_i \frac{1}{2}m\omega^2 r_i^2 \hat{n}_i, \tag{1}$$

where t is the (nearest-neighbor) tunneling energy, i and j are lattice site indices, $\langle i,j\rangle$ represents a sum over nearest neighbors, U is the on-site interaction energy, and $\hat{n}_i = \hat{b}_i^\dagger \hat{b}_i$ gives the number of atoms at site i. The tunneling and interaction energies can be adjusted by tuning the lattice potential depth s, which is controlled by the optical power of the 812 nm lattice light. The parabolic trapping potential with frequency ω provides a spatially varying potential gradient. While the trap is treated as spherically symmetric in Eq. 1., there are three principal axes with different trap frequencies in the experiment.

Potential gradients large enough to produce localization are achieved by using a thermal gas and excluding atoms from the center of the trap by a potential barrier. We access a range of localized states by tuning the lattice potential depth s. By increasing s and thereby reducing t, more particles are localized, since a smaller gradient is required for Stark localization. We characterize the degree of localization by computing the density distribution of the initial state and identifying particles as localized along a lattice direction if the local gradient exceeds the bandwidth $4t$. More details are available in Appendix A. By this measure, 0% (93%) of the atoms are localized along one direction and 0% (80%) are localized along all directions for $s = 4\,\mathrm{E_R}$ ($s = 20\,\mathrm{E_R}$). This lower bound on localization corresponds to atoms confined to a single lattice site. To find an upper bound on localization, we have used exact diagonalization of the one-dimensional single-particle Hamiltonian, and we define delocalized states as those having weight on the central lattice site (as in Ref. [13]). This less stringent upper bound on localization considers a state to be localized if it is excluded from the central (lowest energy) lattice site. For the initial density distribution, all particles are localized by this criterion along at least one direction and 30% (80%) are localized

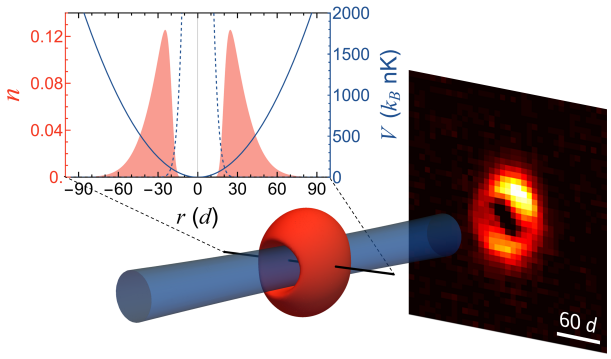

FIG. 1. Procedure to prepare the initial density distribution. After trapping and cooling a thermal gas (red) in a harmonic potential with a repulsive optical potential (blue) present, a cubic optical lattice is slowly turned on. The plot shows the number of atoms per lattice site n for a slice through the predicted density profile (red filled curve) along with the parabolic trapping (solid blue) and barrier (dashed blue) potentials versus position r. A sample column-integrated image taken for the initial state at $s = 10\,\mathrm{E_R}$ is displayed.

in all three directions for $s = 4\,\mathrm{E_R}$ ($s = 20\,\mathrm{E_R}$).

II. STATE PREPARATION

We study dynamics by first creating an equilibrium thermal gas composed of 61 000±6000 atoms confined in an optical dipole trap with a (54.6 ± 0.4) Hz geometric mean trap frequency created with 1064 nm light. The gas is evaporatively cooled in the presence of an optical barrier that excludes atoms from a central region. The barrier is formed from a blue-detuned 766 nm laser beam that is focused backward through the imaging system to a (6 ± 1) µm beam waist. For the measurements discussed here, the optical power is kept fixed, resulting in a barrier with a peak potential of $V = (9000 \pm 5000)\,\mathrm{k_B} \times$ nK. The large uncertainty in the barrier potential does not introduce significant uncertainty in the initial density distribution, since this energy scale is much larger than the (115 ± 10) nK temperature. Given this condition, a hard-wall potential is formed, and the atoms are completely excluded from a cylindrical region with a 14 d radius (where d =406 nm is the lattice spacing) that penetrates through the gas.

After creating a thermal gas, the lattice potential is smoothly ramped on over 100 ms to $s = 4\,\mathrm{E_R}$. The temperature of the gas in the lattice is (210 ± 40) nK, which is determined by fitting the tails of the density distribution (see Appendix B). To study relaxation at higher lattice depths, the lattice potential is quickly increased over 0.4 ms, which is slow enough to avoid band excitation but too fast to allow the density profile to adjust. Therefore, for all data in this paper, the initial density profile is approximately fixed to the distribution realized at $s = 4\,\mathrm{E_R}$.

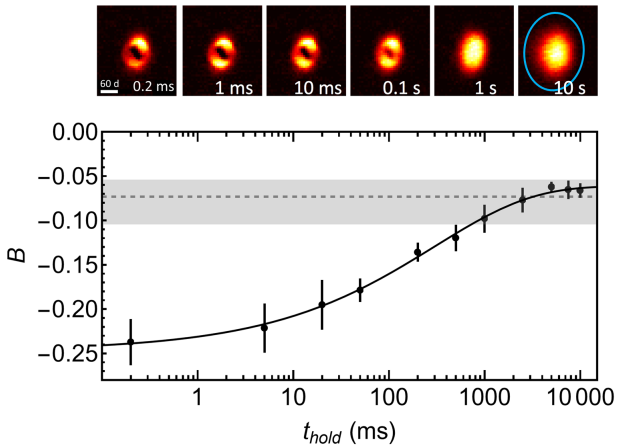

FIG. 2. Relaxation of the density profile. A series of images taken for $s = 7\,\mathrm{E_R}$ is shown, with corresponding measurements of B, for different times after the optical barrier potential is removed. Mardia's B increases towards the equilibrium value over long times as the hole disappears from the density profile. The error bars show the standard deviation for the 4–6 measurements averaged at each hold time. The gray dashed line shows B for a gaussian distribution, and the gray bar displays the range of B values expected for a gas in equilibrium (see Appendix C). The elliptical mask used to suppress the effect of imaging noise is superimposed (light blue) for the image at $t_{hold} = 10$ s. The solid black line is a fit to a stretched exponential. The stretched exponential fit fits the data well for all lattice depths with adjusted R-squared values ranging from 0.87 to 0.97.

The resulting density profile in the lattice is gaussian on the edges of the distribution but has a completely empty region in the center (Fig. 1). To determine the number of atoms per site, we simulated the density distribution using Maxwell-Boltzmann statistics and the atomic limit. A peak density of 0.2 atoms per site occurs just outside the edge of the barrier potential, and the gas has an RMS size of approximately 40 d, which is 30% larger than a gas at the same temperature without the barrier present.

To observe dynamics, we remove the barrier by quickly extinguishing the 766 nm laser beam over 300 µs. The density distribution is allowed to evolve in the trap and lattice potential for a variable time. After this evolution time, an image is taken in situ with variable repumping to control the optical depth and to mitigate imaging artifacts. By partially repumping the gas to the imaging state we operate in a regime well below the maximum optical depth that can be observed.

III. OBSERVATIONS OF DYNAMICS

Typical images for different evolution times are shown in Fig. 2 for $s = 7\,\mathrm{E_R}$. The hole in the density pro-

file disappears over hundreds of milliseconds. We use Mardia's B statistic, which is a kurtosis-like measure of gaussianity, to quantify the dynamical timescale for this change and to determine whether the distribution ultimately achieves equilibrium. Mardia's B is a multivariate measure that is affine-invariant and robust to the overall size, angle, and aspect-ratio of the distribution (which vary over the range of experimental parameters). Unlike other measures that have been used to probe density relaxation in strongly correlated lattice gases [9, 11, 12], Mardia's B is sensitive to the overall shape of the density profile. These features make B an ideal measure for probing relaxation, since the equilibrium thermal density distribution is gaussian for a trapped gas. Mardia's B statistic for an image is determined according to:

$$B = \frac{1}{8}\sum_{i=1} w_i \left[\begin{pmatrix} x_i - \bar{x} & y_i - \bar{y} \end{pmatrix} \hat{\Sigma}^{-1} \begin{pmatrix} x_i - \bar{x} \\ y_i - \bar{y} \end{pmatrix} \right]^2 - 1, \tag{2}$$

where

$$\hat{\Sigma} = \sum_{j=1} w_j \begin{pmatrix} x_j - \bar{x} \\ y_j - \bar{y} \end{pmatrix} \begin{pmatrix} x_j - \bar{x} & y_j - \bar{y} \end{pmatrix}, \tag{3}$$

and w_i is the normalized weight at pixel i, x_i (y_i) is the horizontal (vertical) position of pixel i, and $\bar{x}$ ($\bar{y}$) is the horizontal (vertical) centroid [14]. To suppress the impact of imaging noise, we mask the contribution of pixels at large radii, which introduces a small systematic shift in B for an equilibrium gaussian distribution (see Appendix C). For all lattice depths probed in this work, we find that the time dependence of B fits well to a stretched exponential: $B = B_\infty - A\, e^{-(t_{hold}/\tau)^\beta}$, where t_{hold} is the hold time, B_∞ represents the long-time value of B, τ is a time-constant-like parameter, and β is the stretching exponent (Fig. 2).

Using this method, we observe that equilibrium is achieved at long times for $s = 4 - 20\,\mathrm{E_R}$ (Fig. 3), which includes the regime of complete single-particle localization along at least one lattice direction and nearly complete localization along three directions for all particles. This behavior suggests that Wannier-Stark localization is disrupted, since localization for particles along even one direction would prevent thermalization of the density profile. We have verified that the emergence of a gaussian density distribution at long times is not an artifact of anharmonicity. A simulation of semiclassical dynamics for a system of non-interacting, trapped particles with a lattice dispersion indicates that a detectable remnant of the hole in the density profile persists to long times in the absence of interactions (see Appendix D).

The timescale τ for establishing equilibrium grows with increasing lattice depth and exceeds several seconds at the highest lattice depth, as shown in Fig. 4(a). This trend is consistent with our previous measurements of quasimomentum relaxation [15], which revealed more rapid relaxation at higher lattice depths. Faster relaxation of momentum implies slower equilibration of the density distribution since the self-diffusion constant is proportional to the time-integrated velocity autocorrelation function [16]. The timescale for thermalization τ rapidly increases for $s > 6\,\mathrm{E_R}$, which is the regime for which we observed violation of the Mott-Ioffe-Regel criterion [15]. In this regime, doublon binding and un-binding also become energetically suppressed [17–19], leading to slow dynamics for atoms located on the same site to break apart (and for two separated atoms to tunnel onto the same site).

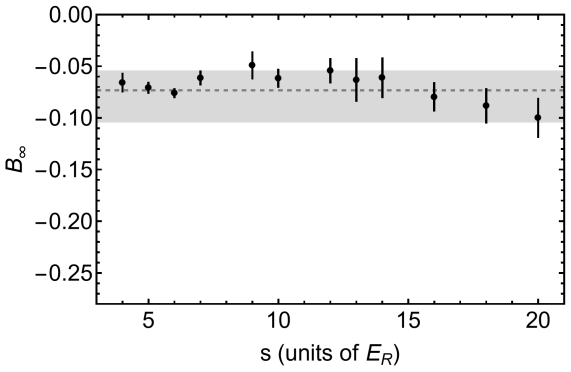

FIG. 3. Long-time value of B determined from stretched-exponential fits such as those shown in Fig. 2. Mardia's B reaches a value consistent with equilibrium for all lattice potential depths s. The error bars show the fit uncertainty. The dashed line shows the value of B for a gaussian distribution (taking into account image masking), and the gray bar is the range of B for an equilibrated gas determined by measurements without the barrier potential present in the initial state.

We also observe that equilibration is non-exponential, except at the highest lattice depths sampled here. Figure 4(b) shows how the stretching exponent β changes with s. The expectation for gases that are weakly interacting or diffusive is exponential relaxation and $\beta = 1$ [16]. However, for $s < 15\,\mathrm{E_R}$, we observe sub-diffusive behavior (i.e., $\beta < 1$), which was also measured in a thermal two-dimensional tilted Fermi-Hubbard system [12] and for a Bose-Einstein condensate confined in a quasiperiodic lattice in the presence of repulsive interactions [20].

Previous theoretical and experimental work has shown that a dramatic slowdown of relaxation and non-exponential behavior can be induced by localization [21–26]. To separate localization from the suppression of tunneling as the lattice depth is increased, we show the measured relaxation time τ normalized to the single-particle characteristic timescale $\hbar/t$ in Fig. 5. The normalized relaxation time approximately follows the fraction of localized particles, which suggests that equilibration is induced by an intrinsic delocalizing effect or interaction with the environment.

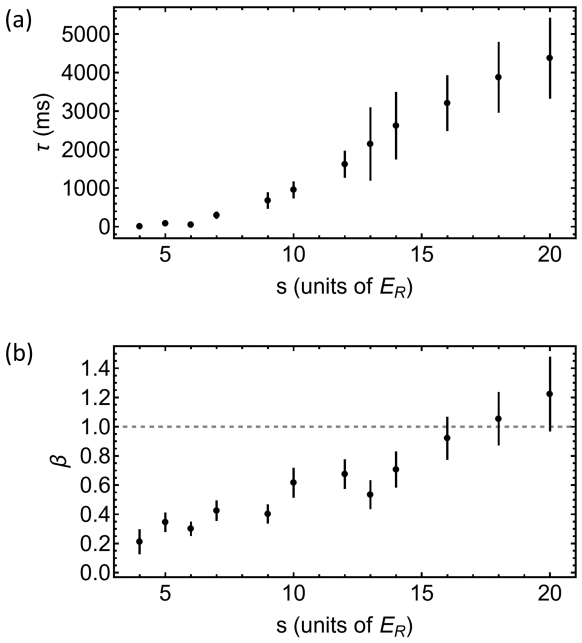

FIG. 4. The relaxation time τ and stretching exponent β determined from fits of B for varied lattice potential depth s. The error bars show the fit uncertainty. (a) The relaxation time rapidly increases above $s = 6\,\mathrm{E_R}$, exceeding several seconds for the highest lattice potential depths. (b) The stretching exponent exhibits non-exponential relaxation for $s < 15\,\mathrm{E_R}$. The dashed line shows agreement with exponential behavior.

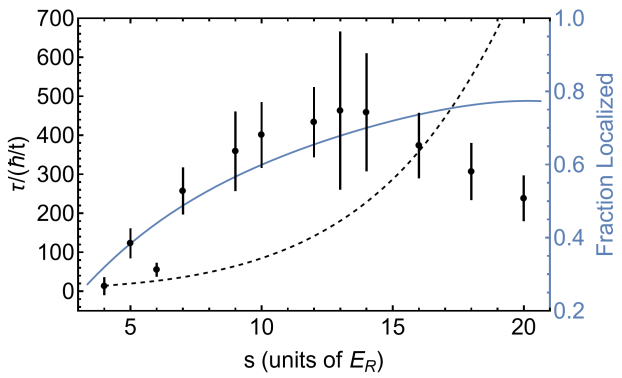

FIG. 5. Relaxation time normalized to the tunneling time $\hbar/t$ for varied lattice potential depths s. The error bars are determined by fit uncertainty. The solid blue line shows the fraction of particles localized in every direction for the initial state, where localization is defined as exclusion from the central lattice site. The dashed black line shows the next-nearest-neighbor tunneling time normalized to $\hbar/t$.

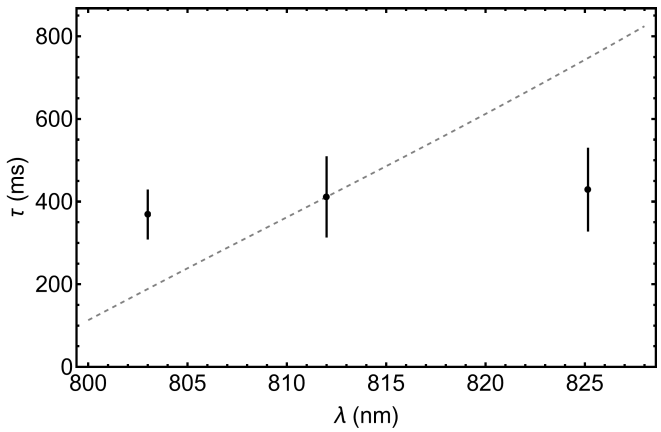

FIG. 6. Relaxation time at $s = 10\,\mathrm{E_R}$ lattice for varied lattice wavelength. The lattice potential depth was kept fixed by tuning the lattice laser optical power. The dashed gray line shows the dependence of the lattice heating rate on wavelength. The error bars are determined by fit uncertainty. Based on a bootstrap analysis, the measured slope (2.9 ± 0.8) ms/nm is inconsistent with the predicted scaling at greater than the 99.99% confidence level.

There are several candidates that may disrupt localization. The most significant interaction effect is the Hubbard energy U, which captures the effect of collisions between particles on the same lattice site. We find that the Hubbard U term does not disrupt localization at the low densities and high lattice depths that we probe here through an exact diagonalization calculation. Interactions reduce the thermally averaged fraction of localized eigenstates for the two-particle Hamiltonian by 20% at $s = 4\,\mathrm{E_R}$. This effect is suppressed at higher lattice depths. For $s = 10\,\mathrm{E_R}$, interactions have a 1% effect, and the effect of U at $s = 20\,\mathrm{E_R}$ is insignificant (see Appendix E).

We also find that heating induced by the lattice light [27], which is the strongest coupling to the environment, is likely not responsible for thermalization. To determine the influence of lattice-light heating, we measured τ at fixed s but different lattice wavelengths (Fig. 6). Across the range we sampled, the heating rate changes by a factor of four, but the measured relaxation time changes by only 15%. We conclude that heating induced by the lattice light is not the dominant source of relaxation. The effects of lattice-light heating on the temperature of the final state is considered in Appendix F. We note that scattering from the 1064 nm optical dipole trap laser light is one-tenth of the scattering from the lattice light at $s = 20\,\mathrm{E_R}$ and is constant across all lattice depths. Therefore, we conclude that scattering from the 1064 nm light is also not a significant source of relaxation.

Atoms in excited bands of the lattice could also play a role in delocalization. We calculated the fraction in the higher energy bands for a gas in a $s = 20\,\mathrm{E_R}$ lattice at the temperature observed at the longest hold time (10 s). We determine that 30% of the atoms are in the first excited band, and 5% are in the second excited band. The bandwidth of the first excited band, $0.24\,\mathrm{E_R}$, is larger than the ground band, but still small relative to the gra-

dient away from the center of the trap. Therefore, approximately 70% of the atoms in the first excited band are localized to a single lattice site. We conclude that excited-band population cannot explain thermalization.

Another source of delocalization and thermalization may be terms beyond the Bose-Hubbard expansion. These represent the full physics of atoms undergoing s-wave collisions in a continuous sinusoidal potential. The largest of these terms is next-nearest-neighbor tunneling. The timescale associated with the next-nearest-neighbor tunneling energy is shown in Fig. 5. Across the range of lattice depths we probe, this timescale is within an order of magnitude of τ, implying that this effect may play a role in equilibration. The timescale associated with the next largest beyond Bose-Hubbard term, nearest-neighbor interactions, corresponds to 90 ms at $s = 4\,\mathrm{E_R}$ and 97 000 ms at $s = 20\,\mathrm{E_R}$, and is therefore likely too small to contribute.

We conclude that a continuum model of interacting lattice bosons may be required to explain the measured thermalization dynamics. These results also highlight the need for more work on understanding thermalization for strongly correlated systems in regimes that involve the interplay of interactions, localization, and constraints such as doublon binding. Furthermore, our results are consistent with previous measurements of slow thermalization for mass transport in the low-temperature regime [28] and have important implications for observing equilibrium physics in optical lattice experiments.

ACKNOWLEDGMENTS

We thank Bryce Gadway for useful discussions regarding interacting Stark localization and exact diagonalization. This work was supported by the National Science Foundation through grant number PHY-2110291.

Appendix A: Localization Estimate

The lower bound on localization was determined by summing the number of atoms on sites where the overall trapping potential gradient is greater than $4t/d$ for the initial state. We carried out this procedure for each direction of the lattice independently. The results are shown in Fig. 7.

To obtain an upper bound on localization, we used exact diagonalization to find the eigenstates of a one-dimensional, single-particle, tight-binding Hamiltonian with a harmonic potential centered on a 300-site lattice. We characterize an eigenstate as delocalized if it has at least 0.1% probability on the central lattice site. The results are not sensitive to the choice of threshold probability. To determine the fraction of atoms localized in the initial state, we project the Wannier state on each lattice site onto the energy eigenstate basis. We average the localized probability on each lattice site weighted by the number density distribution (Fig. 8).

In order to produce an average across the atomic density distribution, we treat the wavefunctions as separable (i.e., products of wavefunctions that depend on one coordinate only). The fraction of the atomic wavefunction that is localized at each site is determined for each direction independently. The measure of the localization fraction for all three directions is calculated by multiplying together the localization fraction in each direction (for

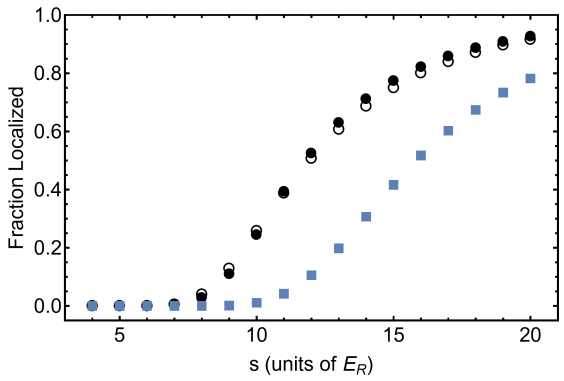

FIG. 7. A lower bound on localization. The blue squares show the fraction of atoms localized to a single lattice site in all three directions. The black circles show the fraction of particles localized along at least one lattice direction. The open and closed circles represent different lattice directions. The slight differences between lattice directions arise because the lattice axes are not aligned to the principal axes of the trap.

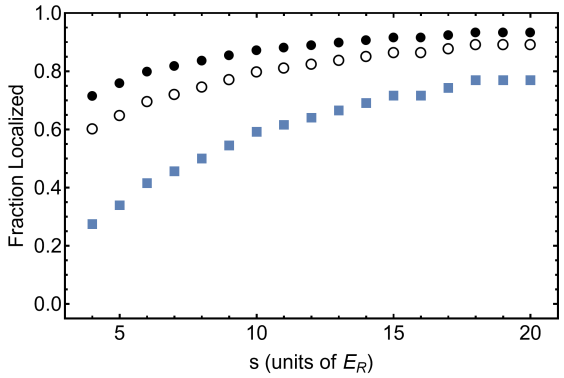

FIG. 8. Upper bound on localization. The blue squares represent the fraction localized in all three directions. The black open circles represent the fraction localized along the direction of the optical barrier propagation and the black filled circles represent the fraction localized along the direction perpendicular to the propagation.

each lattice site). The averages shown in Fig. 8 are calculated using the three-dimensional number-density distribution as a weight.

For this upper bound calculation of localization, we find that approximtely 70% of the particles are localized in at least one direction, even for the lowest lattice depths. The localization fraction increases with lattice depth to a plateau near 95% for the most localized direction (Fig. 8).

Appendix B: Initial Density Distribution

The frequencies of the trap before turning on the lattice were measured by inducing small oscillations. We determined that one principal axis is oriented vertically with frequency (73.9 ± 2.0) Hz and the other two are in the horizontal plane with approximately equal frequencies (48.2 ± 2.0) Hz and (45.7 ± 2.0) Hz. The additional confinement from the lattice beams is included in modeling the density profile. Given systematic uncertainty, we estimate that the lattice beam waist is 120^{+30}_{-10} µm based on the consistency between the lattice beam power, lattice potential depth, and measurements of the forces induced by the envelope of the lattice beams.

The temperature of the initial state (210 ± 40) nK after turning on the lattice was determined by fitting an in-situ image of the gas to a gaussian function. The central region of the gas where the density is excluded by the barrier potential is masked for this fit, so that the temperature is determined by the tails of the density distribution. The temperature measured using this method was checked by entropy matching [29]. Based on an expansion velocity measurement of the temperature (115 ± 10) nK before turning on the lattice, the entropy-matched temperature in the lattice is predicted to be (210 ± 35) nK.

The parameters for the barrier potential were determined by fitting an in-situ image of the gas to a Maxwell-Boltzmann distribution. For this procedure, the overall potential V was modeled as a combination of an attractive harmonic potential and a repulsive potential arising from a focused gaussian laser beam. A measurement of the optical power was used to constrain the magnitude of the barrier potential, leaving just the waist as a free parameter in the fit.

The density distribution of the initial state was modeled via an atomic-limit calculation. The potential energy, including the harmonic confining potential, the barrier potential, and the additional confinement from the $4\,E_R$ lattice beams, was determined for each lattice site. The number of atoms at each site was determined using the potential energy, interaction energy, and measured temperature for a basis of 0–3 particles and a Maxwell-Boltzmann distribution. An overall chemical potential was varied to match the total atom number. We find that 10% of the atoms are on doubly occupied sites for the initial state. The impact of interactions on the density distribution is small—the RMS size of the gas associated with the tails of the density distribution changes by only 2% for $U = 0$.

Appendix C: Mardia's B Statistic

The calculation of Mardia's B statistic is sensitive to imaging noise. To reduce these effects, a defringing technique was applied to the images [30]. Furthermore, a mask was used to calculate B for only the region of the image with sufficient signal-to-noise ratio. The mask was determined by fitting the tails of the distribution to a gaussian in an elliptical coordinate system with the angle of the axes as a free parameter. The mask was applied at three times the RMS radii from this fit. This procedure provides a balance that eliminates nearly all background noise while only introducing a small systematic shift. The shift in B for a gaussian distribution based on this procedure is -0.07, which was determined by applying this procedure to generated images of perfect gaussians. To check the validity of Mardia's B statistic as a measure of equilibrium, we measured B for several equilibrium gases with no barrier potential present. We find that B ranges from -0.10 to -0.05, which is consistent with the value for a masked, ideal gaussian distribution.

Appendix D: Non-Interacting Dynamics

In a harmonically trapped system with a free-particle distribution, the phase-space distribution describing the position and momentum of non-interacting particles rotates at the trap frequency. These dynamics will not lead to relaxation. The dynamics in a system with a lattice dispersion is more complex, and it is possible that dephasing of trajectories could mimic a gaussian density distribution at long times.

To rule out this scenario, we simulate semi-classical dynamics for non-interacting particles with a lattice dispersion confined in a parabolic trap. We work in two dimensions and use a symmetric trap with a frequency corresponding to the geometric mean trap frequency in the experiment. In the simulation, the lattice axes are rotated from the trap axes by 47 degrees; we find that the results are not sensitive to this angle. The initial conditions for 10 000 particles are chosen randomly from a Maxwell-Boltzmann distribution that includes the barrier potential.

Euler's method is used to simulate the motion of each particle according to Newton's equation for time t. Mardia's B statistic is determined for a column-integrated density distribution. The results of this simulation are shown in Fig. 9. To probe dynamics in a system with relatively few localized states, the dynamics are simulated at $s = 4\ E_R$ for 20 nK, which is much lower temperature compared with the experiment, (210 ± 40) nK. For the equilibrium case, the dynamics preserve the initial distribution (Fig. 9(a)). In contrast, initial dynamics

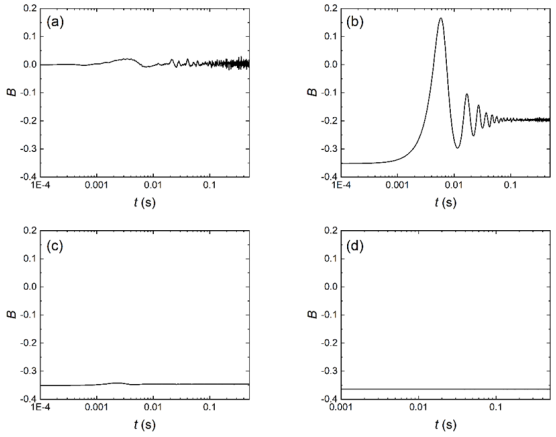

FIG. 9. Simulation of semi-classical dynamics. Two scenarios are simulated at much lower temperature (20 nK) compared with the experiment for $s = 4\,\mathrm{E_R}$: (a) an initial condition at equilibrium and without the barrier and (b) an out-of-equilibrium distribution produced using the barrier potential. Simulations of a 200 nK out-of-equilibrium distribution at $s = 4\,\mathrm{E_R}$ and $s = 20\,\mathrm{E_R}$ are shown in panels (c) and (d).

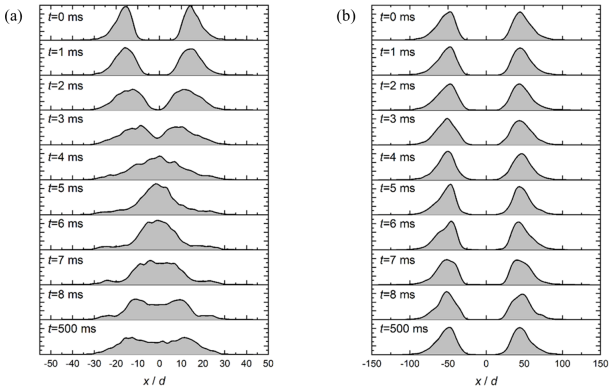

FIG. 10. Simulation of the time-dependent column-integrated density profile for a 20 nK (a) and 200 nK (b) gas.

for the out-of-equilibrium case settle into stationary, but not equilibrium, behavior after approximately 0.1 s (Fig. 9(b)).

The short-time dynamics are suppressed in the higher temperature regime explored by the experiment. Simulations for 200 nK at $s = 4\,\mathrm{E_R}$ and $s = 20\,\mathrm{E_R}$ are shown in panels (c) and (d) of Fig. 9. At these temperatures, a quasi-static distribution is achieved at short times. Furthermore, dynamics present at low lattice depth disappear for stronger lattices.

Snapshots of the column-integrated density profile for 20 nK (Fig. 10(a)) and 200 nK (Fig. 10(b)) at $s = 4\,\mathrm{E_R}$ provide more information about the difference between the low and high-temperature cases. At low temperatures, many particles are free to move, and the short-time dynamics are similar to the free-particle case. Eventually, the lattice dispersion leads to dephasing of particle trajectories and a non-equilibrium stationary density distribution emerges. For higher temperatures or stronger lattices, most of the particles are Stark-localized, motion is not possible, and the initial density distribution is preserved to long times.

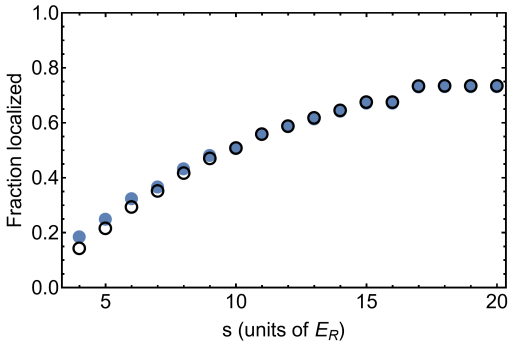

FIG. 11. Fraction of atoms localized for interacting (open, black) and non-interacting (closed, blue) atoms for the equilibrium distribution.

Appendix E: Interaction Effects

We carried out an exact calculation to probe the impact of interactions on localization. We created a set of basis states consisting of all possible configurations of two particles populating a one-dimensional, 60-site lattice centered on a parabolic potential. The Bose-Hubbard Hamiltonian was diagonalized using this set of basis states. We defined eigenstates with less than 0.001% probability on the central lattice site as localized. We determined a localization fraction averaged over the equilibrium distribution by taking the thermal average of the eigenstates at the measured long-time temperature (which depends on s). The results of this calculation vary by less than 10% for a range of 0.0002% to 0.005% in the probability threshold for localization.

We find that interactions modify the localized fraction at low lattice depths but do not affect localization at high lattice depths (Fig. 11). The small influence of interactions may, in part, be due to the relatively small presence of doubly occupied sites. For the final state at $4\,\mathrm{E_R}$ ($20\,\mathrm{E_R}$), we estimate that 5% (2%) of atoms are are located on a doubly occupied site.

Appendix F: Temperature of the Final State

Since removing the potential barrier is diabatic, we expect that the final-state temperature will be larger

compared with the initial state. Furthermore, increasing the lattice potential adds potential energy from added parabolic confinement, and the lattice light heats the atoms.

To check that the final state is consistent with these effects, we calculated the equilibrium temperature by matching the total energy per particle. We used a three-dimensional atomic limit calculation and Maxwell-Boltzmann statistics for a basis involving 0–3 atoms per site. An overall chemical potential was used to match particle number. We computed the energy per particle for the initial state, added the potential energy from increasing the lattice potential depth, and incorporated heating from lattice-light scattering [27]. We determined the final-state temperature needed to match the resulting energy per particle. For a 10-second hold time, we find an expected temperature of (390 ± 40) nK for a $4\,\mathrm{E_R}$ lattice and (1200 ± 120) nK for a $20\,\mathrm{E_R}$ lattice.

We compare the expected temperature to the temperature determined by fitting images obtained at 10 s to a gaussian distribution. At $s = 4\ E_R$, the measured temperature is (390 ± 40) nK, which agrees with our estimate. At $s = 20\ E_R$, the measured temperature of (700 ± 180) nK below our expectation. This discrepancy may be accommodated by atom loss, which can lead to a cooling process that competes with heating. Since atom loss is driven by lattice-light scattering for our experiment (the vacuum-limited lifetime exceeds 5 minutes), this effect will be stronger at higher lattice potential depths. We measure that approximately 40% of the atoms are lost after 10 s at $s = 8\ E_R$.

[1] R. Nandkishore and D. A. Huse, Many-Body Localization and Thermalization in Quantum Statistical Mechanics, Annu. Rev. Condens. Matter Phys. **6**, 15 (2015).

[2] F. Alet and N. Laflorencie, Many-body localization: An introduction and selected topics, C. R. Phys. Quantum Simulation / Simulation Quantique, **19**, 498 (2018).

[3] D. A. Abanin, E. Altman, I. Bloch, and M. Serbyn, Colloquium: Many-body localization, thermalization, and entanglement, Rev. Mod. Phys. **91**, 021001 (2019).

[4] D. Emin and C. F. Hart, Existence of Wannier-Stark localization, Phys. Rev. B **36**, 7353 (1987).

[5] G. Zisling, D. M. Kennes, and Y. Bar Lev, Transport in Stark many-body localized systems, Phys. Rev. B **105**, L140201 (2022).

[6] E. van Nieuwenburg, Y. Baum, and G. Refael, From Bloch oscillations to many-body localization in clean interacting systems, Proc. Natl. Acad. Sci. U.S.A. **116**, 9269 (2019).

[7] M. Schulz, C. A. Hooley, R. Moessner, and F. Pollmann, Stark Many-Body Localization, Phys. Rev. Lett. **122**, 040606 (2019).

[8] E. V. H. Doggen, I. V. Gornyi, and D. G. Polyakov, Many-body localization in a tilted potential in two dimensions, Phys. Rev. B **105**, 134204 (2022).

[9] W. Morong, F. Liu, P. Becker, K. S. Collins, L. Feng, A. Kyprianidis, G. Pagano, T. You, A. V. Gorshkov, and C. Monroe, Observation of Stark many-body localization without disorder, Nature **599**, 393 (2021).

[10] Q. Guo, C. Cheng, H. Li, S. Xu, P. Zhang, Z. Wang, C. Song, W. Liu, W. Ren, H. Dong, R. Mondaini, and H. Wang, Stark Many-Body Localization on a Superconducting Quantum Processor, Phys. Rev. Lett. **127**, 240502 (2021).

[11] S. Scherg, T. Kohlert, P. Sala, F. Pollmann, B. Hebbe Madhusudhana, I. Bloch, and M. Aidelsburger, Observing non-ergodicity due to kinetic constraints in tilted Fermi-Hubbard chains, Nat. Commun. **12**, 4490 (2021).

[12] E. Guardado-Sanchez, A. Morningstar, B. M. Spar, P. T. Brown, D. A. Huse, and W. S. Bakr, Subdiffusion and Heat Transport in a Tilted Two-Dimensional Fermi-Hubbard System, Phys. Rev. X **10**, 011042 (2020).

[13] A. M. Rey, G. Pupillo, C. W. Clark, and C. J. Williams, Ultracold atoms confined in an optical lattice plus parabolic potential: A closed-form approach, Phys. Rev. A **72**, 033616 (2005).

[14] K. V. Mardia, Measures of Multivariate Skewness and Kurtosis with Applications, Biometrika **57**, 519 (1970).

[15] D. Chen, C. Meldgin, P. Russ, B. DeMarco, and E. Mueller, Disappearance of quasiparticles in a Bose lattice gas, Phys. Rev. A **94**, 021601 (2016).

[16] F. Reif, *Fundamentals of Statistical and Thermal Physics* (Waveland Press, 2009).

[17] N. Strohmaier, D. Greif, R. Jördens, L. Tarruell, H. Moritz, T. Esslinger, R. Sensarma, D. Pekker, E. Altman, and E. Demler, Observation of Elastic Doublon Decay in the Fermi-Hubbard Model, Phys. Rev. Lett. **104**, 080401 (2010).

[18] R. Sensarma, D. Pekker, E. Altman, E. Demler, N. Strohmaier, D. Greif, R. Jördens, L. Tarruell, H. Moritz, and T. Esslinger, Lifetime of double occupancies in the Fermi-Hubbard model, Phys. Rev. B **82**, 224302 (2010).

[19] K. Winkler, G. Thalhammer, F. Lang, R. Grimm, J. Hecker Denschlag, A. J. Daley, A. Kantian, H. P. Büchler, and P. Zoller, Repulsively bound atom pairs in an optical lattice, Nature **441**, 853 (2006).

[20] E. Lucioni, B. Deissler, L. Tanzi, G. Roati, M. Zaccanti, M. Modugno, M. Larcher, F. Dalfovo, M. Inguscio, and G. Modugno, Observation of Subdiffusion in a Disordered Interacting System, Phys. Rev. Lett. **106**, 230403 (2011).

[21] A. Signoles, T. Franz, R. Ferracini Alves, M. Gärttner, S. Whitlock, G. Zürn, and M. Weidemüller, Glassy Dynamics in a Disordered Heisenberg Quantum Spin System, Phys. Rev. X **11**, 011011 (2021).

[22] R. Yao and J. Zakrzewski, Many-body localization of bosons in an optical lattice: Dynamics in disorder-free potentials, Phys. Rev. B **102**, 104203 (2020).

[23] R. Harris, Y. Sato, A. J. Berkley, M. Reis, F. Altomare, M. H. Amin, K. Boothby, P. Bunyk, C. Deng, C. Enderud, S. Huang, E. Hoskinson, M. W. Johnson, E. Ladizinsky, N. Ladizinsky, T. Lanting, R. Li, T. Medina, R. Molavi, R. Neufeld, T. Oh, I. Pavlov, I. Perminov, G. Poulin-Lamarre, C. Rich, A. Smirnov, L. Swenson,

N. Tsai, M. Volkmann, J. Whittaker, and J. Yao, Phase transitions in a programmable quantum spin glass simulator, Science **361**, 162 (2018).

[24] H. P. Lüschen, P. Bordia, S. S. Hodgman, M. Schreiber, S. Sarkar, A. J. Daley, M. H. Fischer, E. Altman, I. Bloch, and U. Schneider, Signatures of Many-Body Localization in a Controlled Open Quantum System, Phys. Rev. X **7**, 011034 (2017).

[25] J. Choi, S. Choi, G. Kucsko, P. C. Maurer, B. J. Shields, H. Sumiya, S. Onoda, J. Isoya, E. Demler, F. Jelezko, N. Y. Yao, and M. D. Lukin, Depolarization Dynamics in a Strongly Interacting Solid-State Spin Ensemble, Phys. Rev. Lett. **118**, 093601 (2017).

[26] G. Kucsko, S. Choi, J. Choi, P. C. Maurer, H. Zhou, R. Landig, H. Sumiya, S. Onoda, J. Isoya, F. Jelezko, E. Demler, N. Y. Yao, and M. D. Lukin, Critical Thermalization of a Disordered Dipolar Spin System in Diamond, Phys. Rev. Lett. **121**, 023601 (2018).

[27] D. Mckay, *Quantum Simulation in Strongly Correlated Optical Lattices*, Ph.D. thesis, University of Illinois Urbana-Champaign (2012).

[28] C.-L. Hung, X. Zhang, N. Gemelke, and C. Chin, Slow Mass Transport and Statistical Evolution of an Atomic Gas across the Superfluid–Mott-Insulator Transition, Phys. Rev. Lett. **104**, 160403 (2010).

[29] D. McKay, M. White, and B. DeMarco, Lattice thermodynamics for ultracold atoms, Phys. Rev. A **79**, 063605 (2009).

[30] M. Erhard, *Experimente Mit Mehrkomponentigen Bose-Einstein-Kondensaten*, Ph.D. thesis, Universität Hamburg (2004).